Characterization of the Surface Layer of Integrally Skinned Polyimide Membranes: Relationship with Their Mechanism of Formation

S. PEREZ,[1] E. MERLEN,[1]* E. ROBERT,[1] J. P. COHEN ADDAD,[2] and A. VIALLAT[2]

[1]Institut Français du Pétrole, 1 & 4 Av de Bois Préau, BP 311, 92506 Rueil Malmaison Cedex, France, and [2]Laboratoire de Spectrométrie Physique associé au CNRS, Université Joseph Fourier, Grenoble I, BP 87, 38402 St Martin d'Hères Cedex, France

SYNOPSIS

A series of dense films and membranes was prepared using different processes; their surface morphology was investigated by transmission electron microscopy using the replication technique. On the basis of TEM results, SEM observations of cross sections of membranes and gas-separation properties of membranes, two kinds of membrane morphology are evidenced in relation to their preparation conditions and final properties. The first one gives an ultrafiltration-type membrane. Large nodules are observed on the surface of the membranes. It is suggested that these are formed by liquid–liquid separation that occurs by nucleation and growth of the polymer-rich phase. The second one yields gas-separation-type membranes. No nodules are evident at the surface of these membranes. The skin is formed by a step that concentrates the initial solution. It is followed by the transformation of the solution in the glassy state. Liquid–liquid separation takes place below the first skin layers by nucleation and growth of the polymer-poor phase. © 1993 John Wiley & Sons, Inc.

INTRODUCTION

Gas mixtures can be fractionated by using nonporous polymer membranes that have a selective permeability to a gas. This permeation process relies on a mechanism of dissolution and diffusion of the gas through the macromolecular structure of the polymer. Glassy polymeric materials exhibit a better selectivity for gas separation than do rubbery materials but a rather low permeability[1]; much work has been done to improve their permeability.[2] In spite of the good results obtained in this field, these materials cannot be used in the form of dense films in industrial applications because their productivity is too low. They have to be used in the form of asymmetric membranes. Dense films of polymers have been studied to determine what we call the intrinsic permeability of the polymer.

Asymmetric membranes are generally prepared by a wet-phase inversion process originally developed for reverse osmosis by Loeb and Sourirajan.[3] This process has been widely applied to the preparation of membranes that are used for filtration regimes that go from microfiltration to gas separation, i.e., from a pore-diffusion regime to a permeation regime.

In the field of gas separation, the major challenge was to prepare integrally skinned membranes free of defects and presenting an extremely thin skin (< 100 nm). Therefore, the wet-phase inversion process has been refined into two processes that can be described schematically. The first is the dry/wet phase-inversion process that includes two steps: evaporation of the volatile component of the casting solution (dry-phase inversion) prior to coagulation (wet-phase inversion). According to Pinnau et al.,[4] the important step leading to the formation of extremely thin-skinned membranes is obtaining dry-phase inversion prior to coagulation. Flat-sheet membranes with an apparent skin thickness of less than 50 nm have been prepared recently.[5] The sec-

* To whom correspondence should be addressed.

Journal of Applied Polymer Science, Vol. 47, 1621–1631 (1993)
 CCC 0021-8995/93/091621-11

ond process has been studied by Van't Hoff[6] and consists of a dual coagulation procedure that we identify as a wet/wet process. This procedure is based on the "delayed demixing" behavior of polymer solution in contact with nonsolvents such as high molecular weight alcohols or glycerin.[7] The first step of this process is an immersion of the cast film or the spun extrudate into a nonsolvent of the polymer. The time of immersion is short so that no demixing occurs. During this delay time, there is a large outflow of solvent from the solution while the inflow of nonsolvent is small. The second step is the coagulation of the membrane in a nonsolvent, which results in a phase-inversion phenomenon. This process has been used to obtain hollow-fiber membranes; it has not yet produced integrally skinned membranes having a skin thickness lower than 0.5 μm.

It is thus of a great importance to progress in understanding the phase-inversion mechanism in order to correlate the conditions of preparation, the morphology, and the final properties of the membranes. In a recent paper, Kesting[8] reviewed work on the microscopic characterization of the surface layers of microfiltration (MF), ultrafiltration (UF), reverse osmosis (RO), and gas separation (GS) asymmetric (or integrally skinned) membranes. He identified four tiers of structure levels that can be correlated to the various separation regimes: macromolecules, nodules, nodule aggregates, and superaggregates. The degree of coalescence of these nodular structures would then account for the type of pores in the various separation regimes.

The aim of this study was to characterize the skin microstructure of membranes prepared with the different refinements of the phase-inversion process. Another objective is to attempt to describe the phase-inversion mechanisms to determine the relationships that exist between the casting solution composition, the membrane preparation process, the morphology of membranes, and their gas-separation properties.

EXPERIMENTAL

Materials

Polyetherimide (PEI) ULTEM 1000 was purchased from General Electric. It was used after a heat treatment under vacuum at 150°C for 2 h to remove the absorbed water.

The calculated solubility parameter of this polymer, according to the contribution group method applied to polyimides by Charbonneau[9] is 22.5 $MPa^{1/2}$. Therefore, suitable solvents for membrane formation include aprotic solvents like *N*-methyl pyrrolidone (NMP) and halogenated hydrocarbons such as dichloromethane. In this study, solvents were all of reagent grade and used without further purification.

Gas Permeability Experiments

Pure gas volumetric fluxes through dense films and membranes were obtained by using samples with a surface area equal to 17.4 cm^2; the pressure difference was equal to 0.8 MPa at 25°C. The volumetric fluxes were determined by the pressure buildup in a known volume downstream capacity. This volume was adjusted so that the pressure buildup was kept low relative to the pressure difference between the upstream and downstream sides of the sample.

The flux of the gas i is:

$$J_i = P_i A \Delta p / e \quad (1)$$

where A and e are, respectively, the surface area and the thickness of either the dense film or the separating layer of the membrane; Δp, the pressure difference between the upstream and the downstream sides of the sample; and P_i, the intrinsic permeability of the polymer for the gas i. The measure of the flux J_i through dense films with a known surface area and a given thickness gives the intrinsic permeability P_i. It is conveniently expressed in barrers (10^{-10} N cm^3 cm/cm^2 s cmHg). In the case of membranes, the thickness of the separation layer is unknown; the measure of the flux gives the permeability of the membrane $(P/e)_i$. Membrane permeability is therefore conveniently expressed in 10^{-6} N cm^3/cm^2 s cmHg.

The ideal selectivity for the separation of two gases denoted i and j is defined for a dense film as the pure gas intrinsic permeability ratio:

$$\alpha_{i/j} = P_i / P_j \quad (2)$$

whereas for a membrane, it is given by the ratio:

$$\alpha_{i/j} = (P/e)_i / (P/e)_j \quad (3)$$

Preparation of Dense Films

Dense films were prepared from solutions of PEI in dichloromethane (DCM) or NMP (see Table I). Films were cast on a glass plate using a doctor blade,

Table I Casting Solution Composition and Temperature of Solvent Evaporation Used for Preparation of Dense Films

Dense Film	Casting Solution (Wt %)	Temperature (°C)
DD16L	PEI/DCM 16/84	35
DD16R	PEI/DCM 16/84	120
ND16L	PEI/NMP 16/84	120
ND30L	PEI/NMP 30/70	120

and the solvent was evaporated to completion: the initial thickness of the films was 150 microns.

The permeability to H_2 and CH_4 was measured only on dense films obtained from NMP solutions. The films obtained from DCM solutions were not tested because of their poor mechanical strength. The intrinsic permeability of ULTEM measured to H_2 is 3.46 barrers and the selectivity to H_2/CH_4 separation estimated from permeability to pure gases is 477.

Preparation of Membranes

Flat membranes were cast using the procedure described for the preparation of dense films. The three types of phase-inversion process mentioned in the Introduction were applied depending on the casting solution composition. Coagulation was also induced by introduction of nonsolvent in the vapor phase. The conditions of preparation of membranes are reported in Table II.

The membrane prepared by a dry/wet process was made according to the conditions described by Pinnau et al.[4] The casting solution was one of those described in the patent literature[10]: It contains dichloromethane, 1,1,2-trichloroethane, xylene, and acetic acid. In this study, the resulting membrane is called REF membrane.

The membranes prepared from a wet process or a wet/wet process were all obtained from solutions of PEI in NMP. Immediately after casting, the films of PEI in NMP were immersed in the nonsolvent bath. In the case of the wet/wet process, after some residence time in the first nonsolvent bath, the film was transferred into the second nonsolvent bath. As is mentioned by Van't Hoff,[6] it is experimentally difficult to bring a film from the first to the second nonsolvent bath.

After a residence time of 10 min in the coagulation bath, or in the case of the wet/wet process, after a residence time of 30 min in the second coagulation bath, all membranes were transferred into a methanol bath for 1 week and then dried at 50°C; they were subsequently heat-treated at 200°C for 2 h under nitrogen.

Gas-separation properties of the membranes (permeability to H_2 and selectivity to H_2/CH_4 separation) are reported in Table III. The permselectivity properties of membranes 4A30 and 5A30 were

Table II Casting Solution Composition and Coagulation Process Used for Membrane Preparation

Membrane	Process	Solution	Coagulant
REF	Dry/wet	PEI 15.9, Dichloromethane 54.6, 1,1,2-Trichloroethane 4.8, Xylene 17.6, Acetic acid 7.1	Acetone
1A16	Wet	PEI 16, NMP 84	Water
1A30	Wet	PEI 30, NMP 70	Water
2A30	Wet	PEI 30, NMP 70	Water/NMP 50/50 wt/wt
3A30	Wet	PEI 30, NMP 70	1-Propanol
4A30	Wet/wet	PEI 30, NMP 70	First: glycerin Second: water
5A30	Vapor	PEI 30, NMP 70	Steam

Table III Gas Separation Properties of ULTEM Membranes

	Permeability to H_2[a]		Selectivity H_2/CH_4[b]	
Membrane	Average	SD	Average	SD
REF	6.5		200	
1A16	115	66	2.7	0.2
1A30	2.3	0.3	80	31
2A30	0.65	0.07	49	16
3A30	0.19	0.03	362	74

[a] 10^{-6} cm^3/cm^2 s cmHg.
[b] Obtained from permeability measurements on pure gases at 25°C and ΔP = 0.8 MPa.

not measured because of the nonflatness of these membranes.

The selectivity of membranes cast from ULTEM/NMP solutions vary from 2.7 (Knudsen diffusion) to 362; the latter value is not far from the intrinsic selectivity of the polymer. However, this increase of selectivity is accompanied by a drastic decrease of the permeability. The best compromise combining permeability and selectivity is offered by the REF membrane. Within this study, this membrane will be considered as a reference for gas separation.

Scanning Electron Microscopy

Cross sections of the samples were examined using a JEOL JSM 35 CF. Samples were immersed and broken in liquid nitrogen before being coated with gold.

Transmission Electron Microscopy

Observations were conducted on a JEOL 120 CX used at 100 kV on replicas obtained as follows:

- Sample shadowed with Pt—C at an angle of 25° (~ 5 nm).
- Deposition of a thin amorphous carbon layer (~ 15 nm).
- Deposition of a drop of a 6.2% wt solution of polyacrylic acid.
- Dissolution of the membrane in chloroform.
- Dissolution of the polyacrylic acid in water. This step is performed after immersion of the replica in benzotril. Without the benzonitril immersion, we have observed a systematic destruction of the replica.
- Deposition of the replica on a copper grid.

A replica of a freshly cleaved mica was made to determine the limit of the technique. With low Pt—C coverage, small Pt particles 2–3 nm in size are visualized. When increasing this coverage to reveal the topology of the surface, small 6 nm protuberances appear, giving the limit of this technique.

STRUCTURAL OBSERVATIONS

In this section, the surfaces and the bulk structures of membranes and dense films are analyzed using electron microscopy.

Bulk Structure

Scanning electron microscopy (SEM) is used to probe the bulk structures of the obtained membranes. SEM images shown in Figures 1 and 2 illustrate the two main types of substructures observed in all the membranes studied in this work.

Figure 1(a) and (b) shows, respectively, cross sections of membranes 1A16 and 1A30 both obtained from water coagulation of ULTEM/NMP solutions. Enlargements of the sublayers just below the surface of these membranes are presented on Figure 1(c) and (d).

The porous substructure is characterized by the following:

(i) The presence of macrovoids, also called "fingerlike cavities," that extend from the near surface of the membrane through the whole section of the membrane in the system 1A16 and through about half of the section for membrane 1A30 [Fig. 1(a) and (b)].
(ii) The nodular structure of the polymeric matrix that can be described in terms of spherical particles of 200 and 150 nm diameter for membranes 1A16 and 1A30, respectively, [Fig. 1(c) and (d)].

Figure 2 shows cross sections of membranes REF and 3A30 [Fig. 2(a) and (b)] as well as enlargements of the sublayers located just below the surface [Fig. 2(c) and (d)]. The main characteristic of these two membranes is the existence of a partially interconnected "spongelike substructure"; at this scale of observation, no spherical particles exist in the polymeric matrix. This observation applies to all membranes of this study, except for membranes 1A16 and 1A30.

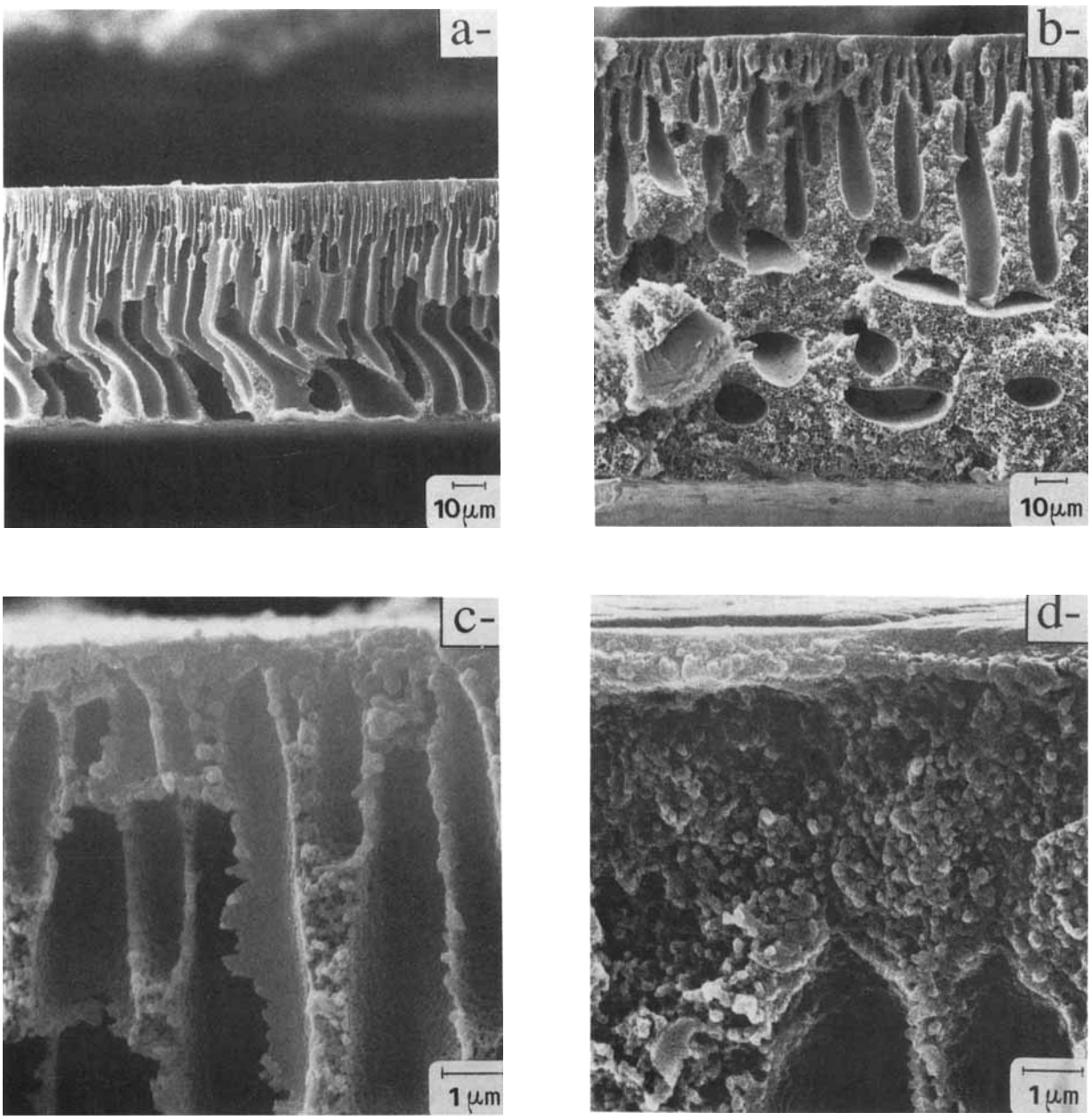

Figure 1 Scanning electron micrographs of the cross section of (a,c) membrane 1A16 and (b,d) membrane 1A30.

Surface Structure

Spherical protuberances are revealed from TEM observations of the replica of the skin surface of all membranes. For membranes 1A16 and 1A30, the average diameters can be measured perpendicularly to the shadowing direction. For the other membranes and for the dense films, no quantitative description of the size of the protuberances detected on these surfaces can be given; 6 nm is the limit of our experimental method.

Figure 3 shows a micrograph obtained for the membrane REF. It is taken as a membrane of reference because of its rather good permselective properties (see Experimental). The surface topology of this membrane consists of a well-defined distribution of protuberance sizes ranging between 6 and 9 nm, which is near the limit for this shadowing method. So, it is difficult to conclude on the presence of small protuberances for this kind of membrane.

The study of the micrographs obtained for all other membranes made from ULTEM/NMP so-

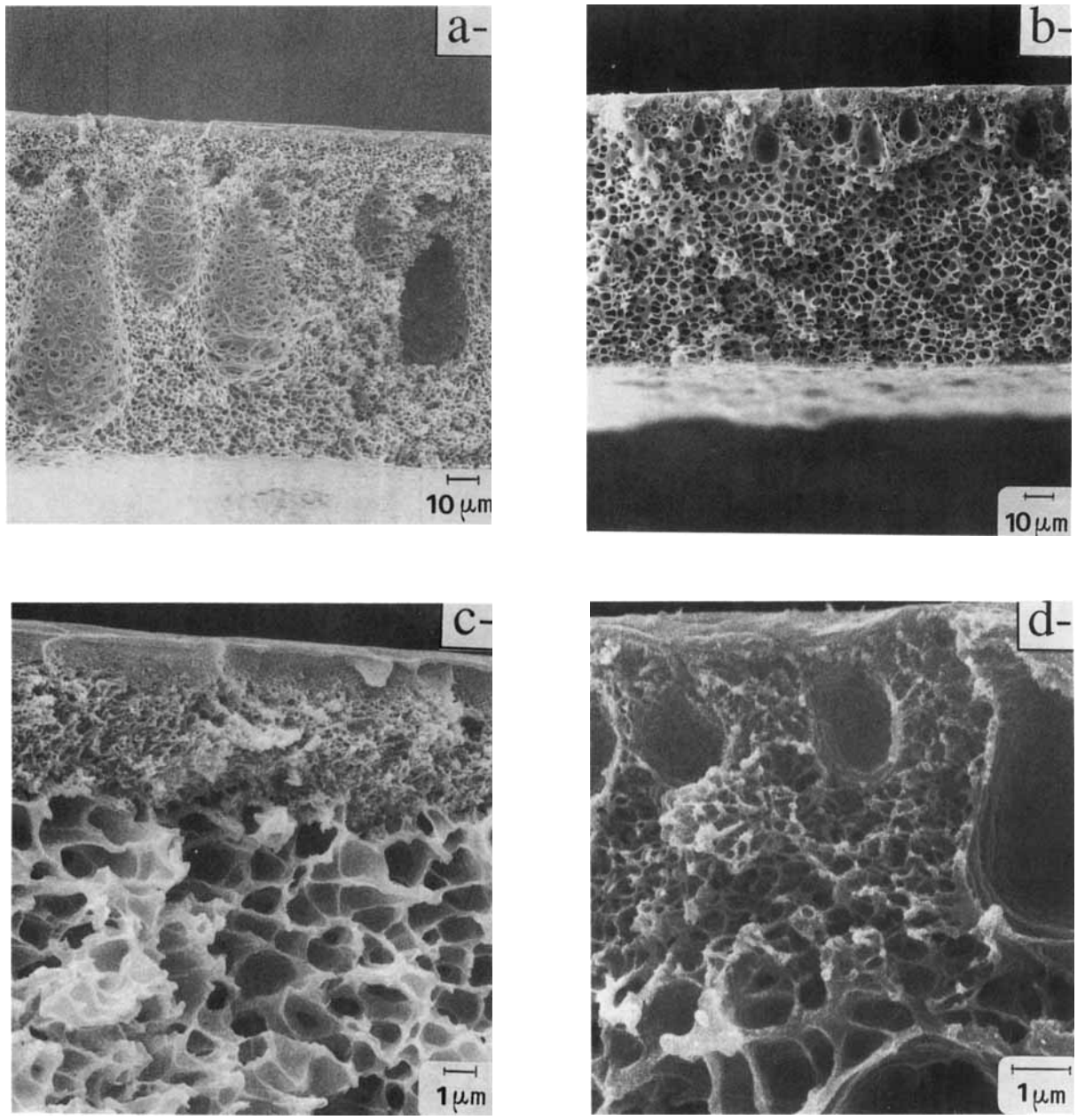

Figure 2 Scanning electron micrographs of the cross section of (a,c) membrane REF and (b,d) membrane 3A30.

lutions brings out the fact that there are two kinds of surface topology. This is illustrated with micrographs of Figure 4(a) and (b) obtained, respectively, for membranes 1A16 and 3A30. In these figures, the spherical protuberances observed at the surface of membrane 1A16 are much larger than those observed at the surface of the reference membrane (Fig. 3). However, in the case of membrane 3A30, the protuberances observed are again at the limit of resolution. Thus, the surface topology can be modified by varying the conditions of formation of the membrane. This is illustrated in the following way:

(i) The evolution of the surface topology was first studied as a function of the polymer concentration. Figure 4(a) and (c) shows that the average diameter of the protuberances decreases as the polymer concentration increases. The average diameter measured at the surface of membrane 1A30 is

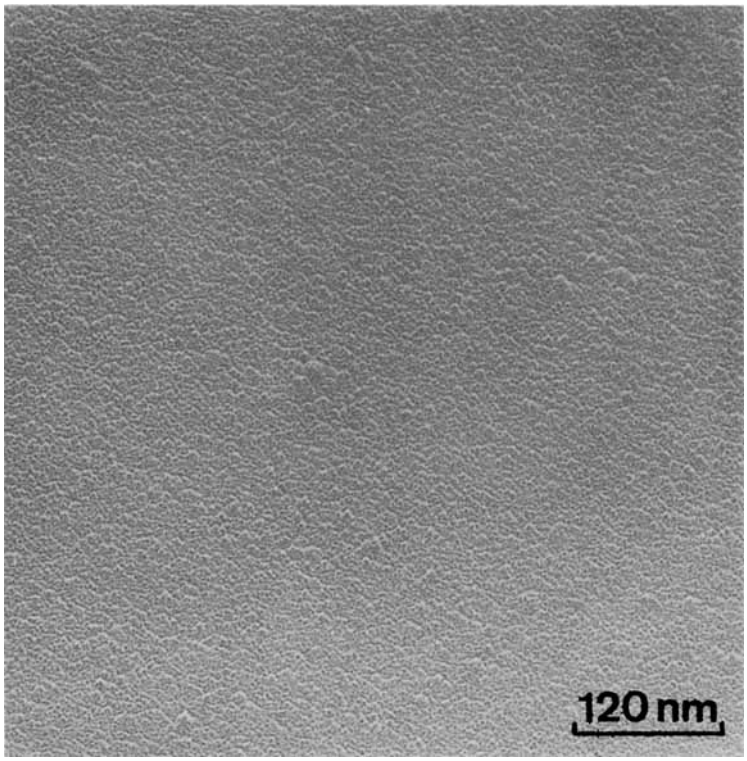

Figure 3 Electron micrograph of Pt—C preshadowed replica of the surface of a gas-separation membrane (membrane REF).

equal to 18 nm, whereas it is equal to 36 nm for membrane 1A16.

(ii) The effect of the nature of the nonsolvent was also studied. The largest protuberances were obtained for membranes 1A16 and 1A30 made by water-immersion coagulation. The superficial topology of membrane 2A30 obtained with a binary coagulant water/NMP is coarse [Fig. 4(d)], whereas membrane 3A30, formed with the coagulant propanol, shows, as the membrane REF, a topology at the limit of resolution [Fig. 4(b)]. For membrane 4A30 (micrograph not shown) made first using glycerin and, second, using water as coagulants, the results obtained are similar to those found on membrane 3A30. However, a few protuberances, 30 nm in size, have been observed.

(iii) The effect of the coagulation process (coagulation by immersion in water or under steam) was studied for one particular solvent (NMP) using two polymer concentrations (16 and 30% of ULTEM 1000). Coagulation by immersion in water (membranes 1A16 and 1A30) produces large protuberances on the membrane surface, whereas coagulation under steam (membrane 5A30, micrograph not shown) leads to a membrane with a superficial topology similar to the one of the reference membrane (Fig. 3).

In the case of dense films, the influences of the solvent evaporation rate and of the polymer concentration in the initial solution have been checked both for ULTEM/NMP and ULTEM/DCM solutions. Figure 5(a) and (b) was obtained, respectively, for DD16L and ND30L films. The micrographs always show the presence of small protuberances (<6 nm) on the surface, which are, again, at the limit of resolution.

The dense films DD16L and ND30L were prepared from initial solutions comparable to those used in the formation of the membranes REF (ULTEM in DCM) and 3A30 (ULTEM in NMP), respectively. The surface topology of the membrane REF (Fig. 3) and of the membrane 3A30 [Fig. 4(b)] are comparable to those of the dense films DD16L [Fig. 5(a)] and ND30L [Fig. 5(b)].

Finally, on the one hand, the examination of the porous substructure and, on the other hand, the comparison of the surfaces of dense films and mem-

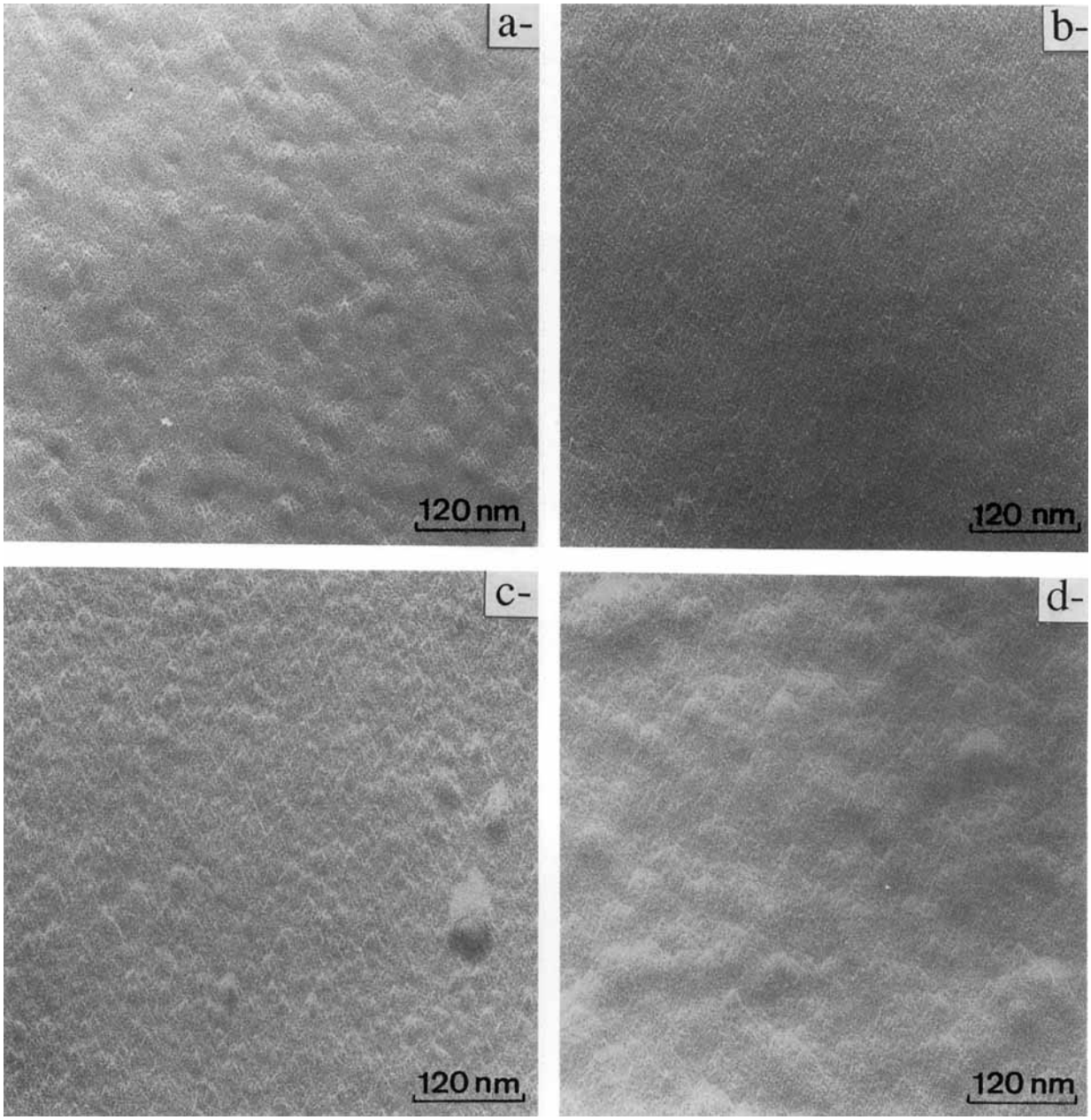

Figure 4 Electron micrograph of Pt—C preshadowed replicas of the surface of membranes (a) 1A16, (b) 3A30, (c) 1A30, and (d) 2A30.

branes suggest the existence of two different mechanisms of formation of these two types of surface topology.

DISCUSSION—TWO POSSIBLE MECHANISMS

The discussion concerns the two kinds of membranes evidenced in the foregoing section. The following analysis is now proposed to attempt to interpret the formation of these membranes:

The first kind of membrane is obtained by a wet process using water or water/NMP as a coagulation medium. It is of an ultrafiltration (UF) type and shows both a skin and a substructure composed of nodules in the range from 18 to 36 nm for the skin layer and from 150 to 200 nm for the substructure. The second type of membrane is obtained either by a dry/wet process or a wet or wet/wet process using

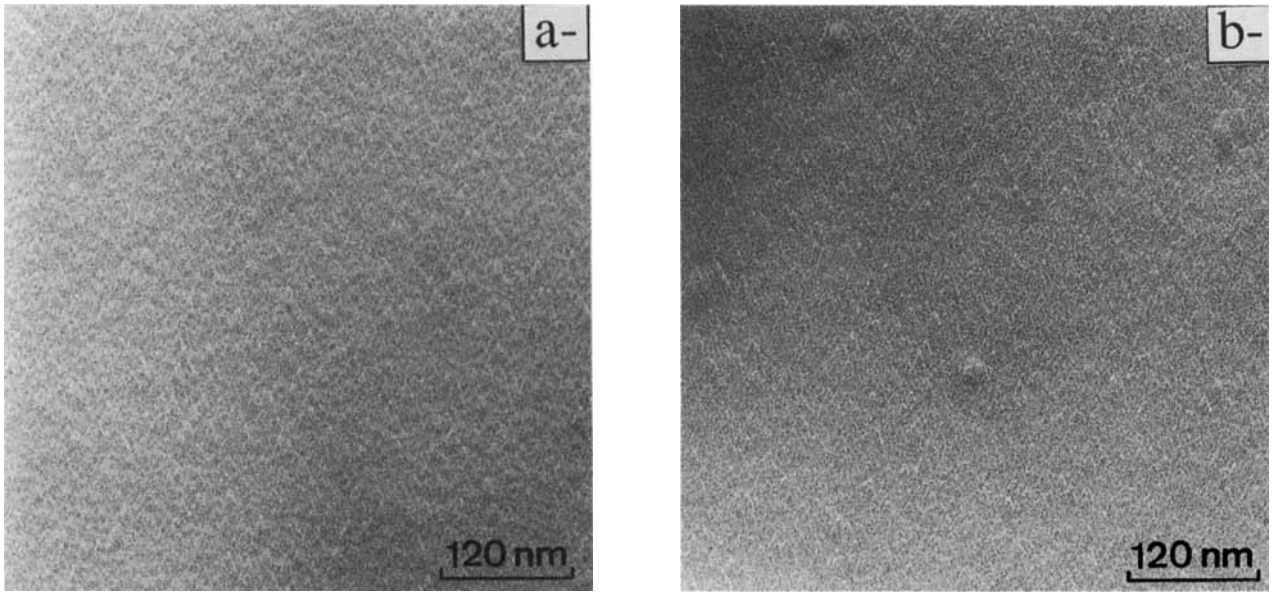

Figure 5 Electron micrograph of Pt—C preshadowed replicas of the surface of dense films (a) DD16L and (b) ND30L.

high molecular weight alcohols or glycerin as a first coagulation medium. The skin structure of these latter membranes, classified as gas-separation (GS) membranes, seems identical to those observed either on membranes obtained from coagulation by introduction of water vapor or on dense films.

The existence of nodules on surface membranes has been previously reported.[11–16] All studies show that the size of nodules varies from 18 to 200 nm. The presence of these nodular structures has been identified as being related to the formation of membranes according to the mechanism that was first proposed by Maier and Scheuermann.[17] The initial homogeneous polymer solution is transformed into a dispersed phase of micelles in a polymer-poor phase. But this mechanism is valid only when the polymer concentration is lower than the critical solution concentration. However, the critical point in polymer solutions is generally located at polymer concentrations lower than 10%, obviously lower than the concentrations used for membrane preparation. Thus, Broens et al.[15] considered that in the case of cellulose acetate, polyacrylonitrile, polydimethylphenylene oxide, and polysulfone the liquid–liquid separation in the phase-inversion process can take place only through nucleation and growth of a polymer-poor phase. Therefore, liquid–liquid separation cannot explain the existence of a nodular structure. These authors have then proposed that these nodules were due to the formation of an "ordered phase of polymer."

The possibility to distinguish two mechanisms involved in the formation of UF and GS membranes is now discussed by taking results reported previously into consideration.

Qualitative Description of the Formation of UF Membranes

It has been shown in recent studies described elsewhere[18,19] that two features characterize ULTEM/NMP solutions. The first one concerns the formation of polymer–polymer associations. This is probably due to the presence of intermolecular charge-transfer complexes. Polymer aggregation is enhanced by the presence of water in ULTEM/NMP solutions. The second feature concerns the influence of association on the form of the binodal curves. These are obtained from cloud-point measurements performed in pseudobinary mixtures. A shift of the precipitation threshold toward great values of the polymer concentration is observed. A polymer–polymer association effect is introduced in a model based on the Flory–Huggins theory of polymer solutions to account for this effect.

As a consequence of the enhancement of polymer-specific association induced by the addition of water to NMP, the following features about the formation of membranes might be predicted:

(i) The inflow of nonsolvent induces a shift of the precipitation threshold toward high values of polymer concentration. Conse-

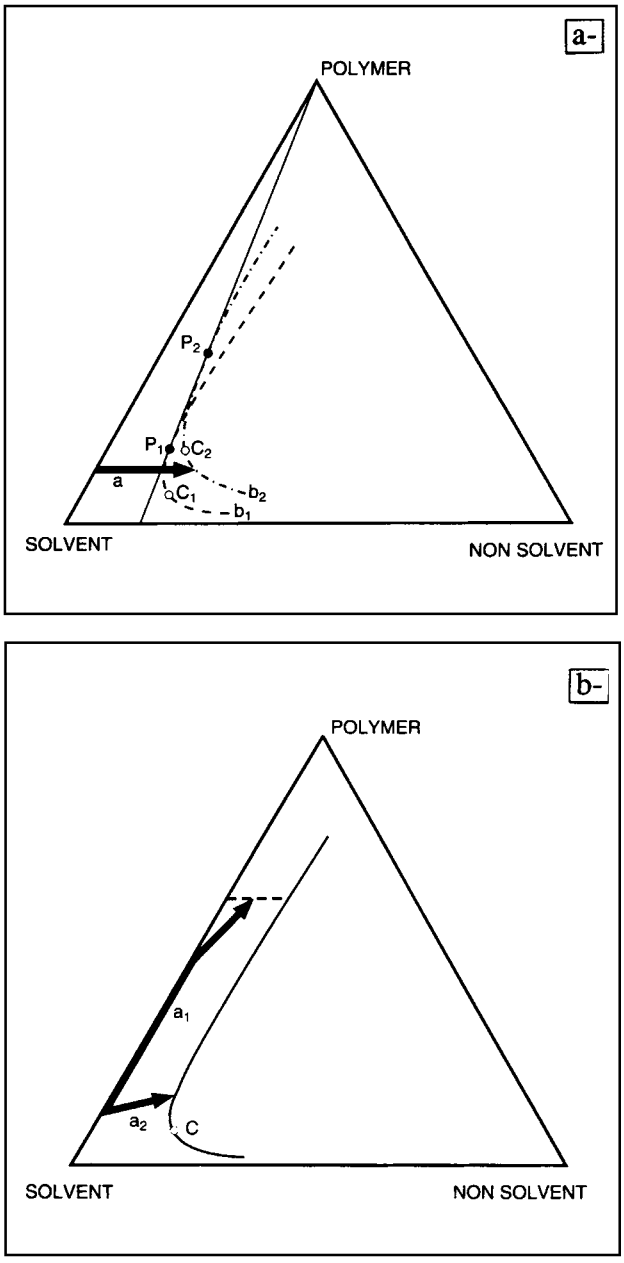

Figure 6 (a) Schematic representation of a ternary phase diagram for the formation of UF membranes. b_1/b_2 is a possible modification of the binodal shape with the inflow of nonsolvent; a is a possible coagulation path; P_1 and P_2 are the precipitation thresholds; and C_1 and C_2 are the critical points for b_1 and b_2 binodals. (b) Schematic representation of a ternary phase diagram for the formation of GS membranes. a_1 and a_2 are possible coagulation paths of, respectively, the skin layer and the sublayers; C is the critical point. (- - -) Sol–gel transition or glass transition.

quently, as is shown in Figure 6(a), the binodal curve also shifts in the same way.

(ii) The composition path of the solution should be reported on a sequence of transient-phase diagrams that results from the modification of the position of the binodal curve [Fig. 6(a)].

(iii) The composition path can therefore penetrate into the demixing domain in a zone corresponding to polymer concentrations lower than the critical concentration.

(iv) Then, liquid–liquid separation can occur by nucleation and growth of a polymer-rich phase in accordance with the mechanism proposed by Maier and Scheuermann.

(v) The resulting structure consists of large nodules that correspond to the polymer-rich phase; they can be partially coalesced.

(vi) According to the frame proposed by Gröbe et al.[20] and Broens et al.,[15] the fingerlike cavities existing in the substructure of the membrane are developed from the polymer-poor phase. The driving force for the growth of fingerlike cavities is supposed to be the strong osmotic pressure that results from the great affinity between solvent and nonsolvent. This induces the propagation of an unstable coagulation front that gives rise to such fingerlike cavities. When solvent is added in the coagulation bath, the osmotic pressure is reduced and, accordingly, the number and the size of fingerlike cavities decrease (membrane 2A30). In agreement with this description, it has been reported elsewhere[21] that the coagulation rate decreases upon addition of NMP in the bath of water.

Qualitative Description of the Formation of GS Membranes

The surface topology of GS membranes is similar to the surface of dense films. During the formation of dense films, the solvent evaporation induces an increase of the concentration of polymer. This leads first to the gelation of the solution and then to its transformation in the glassy state. It is supposed in this work that a similar process occurs during the formation of the skin layer of the GS membranes.

The composition paths followed by the polymer solution after the immersion in a nonsolvent bath[22] are schematically represented in Figure 6(b). The formed dense layer constitutes a barrier both to the outflow of solvent and to the inflow of the non-solvent. Consequently, as is shown in Figure 6(b), the polymer concentration below the skin layer is much lower than the one at the surface of the film. This concentration is comparable to the concentration of

the initial solution and is more than the critical concentration. Then, the liquid–liquid separation can take place by nucleation and growth of a polymer-poor phase. A resulting spongy substructure is observed. The polymer-poor phase constitutes the pores of the substructure. The solid matrix is the polymer-rich phase that has been fixed in the glassy state. Furthermore, very few fingerlike cavities are observed in membranes that were obtained by immersion of ULTEM–NMP solution in 1-propanol (membrane 3A30); no fingerlike cavity exists in membranes made from immersion in glycerin prior to water coagulation (membrane 4A30). In both cases, the coagulation rates are much slower than the one obtained from precipitation of ULTEM–NMP solution in water.[21] The coagulation front becomes progressively stable when the coagulation rate decreases.

The influence of the rate of coagulation was also investigated when the phase inversion was induced by arrival of nonsolvent in the vapor phase. In this process, the nonsolvent diffuses very slowly into the polymer solution and there is almost no solvent outflow. The composition path of the solution is similar to the one drawn in Figure 6(b) for the sublayer of a GS membrane; the liquid–liquid separation occurs by nucleation and growth of a polymer-poor phase in the volume of the solution. As a result, a spongy structure is obtained with almost no gradient of porosity. The topology of the surface is comparable to those observed in the case of dense films.

CONCLUSION

The morphology of membranes govern their final properties. To control these properties, it is crucial to understand the process of formation of these asymmetric structures. It is of a complex nature because it involves competitive kinetics of various thermodynamic phenomena. These can be polymer aggregation, liquid–liquid separation, gelation, and glass transition. This work was focused on the characterization of membrane morphology with regard to conditions of preparation. Particular attention was given to TEM characterization of the membrane surface. Two kinds of surface topology were evidenced. The first one is characterized by the existence of large nodules (> 18 nm); in the second type of surface topology, there is no evidence for the presence of nodules.

A correlation between the nature of the surface topology and the type of the membrane was suggested. The absence of nodules is associated with the type of GS membranes, whereas larges nodules give the UF kind of membranes.

We wish to thank P. Dascotte for his collaboration on preparation and examination of membrane replicas. We are grateful to M. C. Lynch and Dr. E. Rosenberg for their helpful work on the SEM.

REFERENCES

1. J. H. Petropoulos, *J. Memb. Sci.*, **53**, 229–258 (1990).
2. W. J. Koros and M. W. Hellums, *Fluid Phase Equilibria*, **53**, 339–354 (1989).
3. S. Loeb and S. Sourirajan, *Adv. Chem. Ser.*, **38**, 117 (1962).
4. I. Pinnau, J. Wind, and K. V. Peinemann, *Ind. Eng. Chem. Res.*, **29**, 2028–2032 (1990).
5. I. Pinnau and W. J. Koros, U.S. Pat. 4,902,422 (1990).
6. J. A. Van't Hoff, PhD Thesis, Twente University, The Netherlands, 1988, Chap. 4.
7. B. Reuvers, PhD Thesis, Twente University, The Netherlands, 1987.
8. R. E. Kesting, *J. Appl. Polym. Sci.*, **41**, 2739–2752 (1990).
9. L. F. Charbonneau, *J. Polym. Sci. Polym. Chem Ed.*, **16**, 197 (1978).
10. K. V. Peinemann, U.S. Pat. 4,673,418 (1987).
11. R. Shultz and S. Asunmaa, *Rec. Prog. Surf. Sci.*, **3**, 291 (1970).
12. R. E. Kesting, *J. Appl. Polym. Sci.*, **17**, 1771 (1973).
13. M. Panar, H. Hoehn, and R. Hebert, *Macromolecules*, **6**, 777 (1973).
14. I. Cabasso, *Synthetic Membranes*, ACS Symposium Series 153, A. F. Tubbak, Ed., American Chemical Society, Washington, DC, 1981, Vol. 1, Chap. 19.
15. L. Broens, F. W. Altena, C. A. Smolders, and D. M. Koenhen, *Desalination*, **32**, 33–45 (1980).
16. M. N. Sarbolouki, *J. Appl. Polym. Sci.*, **29**, 743–753 (1984).
17. K. H. Maier and E. A. Scheuermann, *Kolloid Z.*, **171**, 122 (1960).
18. A. Viallat, R. Pedro Bom, J. P. Cohen Addad, and S. Perez, to appear.
19. A. Viallat, J. P. Cohen Addad, R. Pedro Bom, and S. Perez, *Polymer*, to appear.
20. V. Gröbe, G. Mann, and G. Duwe, *Faserfors. und Textiltechn.*, **17**, 142 (1966).
21. S. Perez, PhD Thesis, University Pierre et Marie Curie, Paris VI, France, 1991.
22. J. G. Wijmans, J. P. B. Baaj, and C. A. Smolders, *J. Membr. Sci.*, **14**, 263–274 (1983).

Received October 2, 1991
Accepted May 13, 1992